Author Query Form

Journal Title: Proceedings of the Institution of Mechanical Engineers, Part E: Journal of Process Mechanical Engineering [PIE]

Article Number: 539940

Dear Author/Editor,
Greetings, and thank you for publishing with SAGE. Your article has been copyedited and typeset, and if we have any queries for you they are listed below. Please address these queries when you return your proof corrections. Thank you for your time and effort.

Please ensure that you have obtained and enclosed all necessary permissions for the reproduction of artistic works, (e.g. illustrations, photographs, charts, maps, other visual material, etc.) not owned by yourself, and ensure that the Contribution contains no unlawful statements and does not infringe any rights of others, and agree to indemnify the Publisher, SAGE Publications Ltd, against any claims in respect of the above warranties and that you agree that the Conditions of Publication form part of the Publishing Agreement.

Any colour figures have been incorporated for the on-line version only. Colour printing in the journal must be arranged with the Production Editor, please refer to the figure colour policy outlined in the e-mail.

Please assist us by clarifying the following queries:

1. Please check the sentence 'The stated variation is that from...' for clarity.
2. Please provide publisher location for Ref. 1.
3. Please provide publisher location for Ref. 16. Also confirm whether the reference is OK as edited.
4. Please confirm whether the captions of Figures 2 and 12 are correct as set.
5. Please provide expansion for ID (Table 1)

Original Article

Institution of MECHANICAL ENGINEERS

Journal of PROCESS MECHANICAL ENGINEERING

Proc IMechE Part E:
J Process Mechanical Engineering
0(0) 1–14

DOI: 10.1177/0954408914539940
uk.sagepub.com/jpme

SAGE

Experimental and computational analysis of the feed accelerator for a decanter centrifuge

George RA Bell and John R Pearse

Abstract

Industrial decanter centrifuges are used in a wide range of industries to separate mixtures of solids and liquids. One of the main elements of these devices is the feed accelerator, which accelerates the incoming mixture to the high rotational speed required for separation. A well-designed feed accelerator can increase product throughput, solids recovery, and liquid clarity, while a poorly designed accelerator can increase wear and reduce the overall efficiency of the machine. This article presents experimental and computational quantification of the performance of six feed accelerator designs that are currently used in decanter centrifuges. The experimental method allowed for the measurement of accelerator and pool speed efficiencies, and high-speed photography of the flow in the annular space between the accelerator and the rotating pool. The computational model allowed for prediction of the flow path in the annular space and the torque imparted on the fluid by the accelerator. A parametric study was conducted using the aforementioned computational model for drum and disk accelerators. It was found that several of the accelerator design parameters were critical to the overall performance, reinforcing the need for an optimised design. It was found that increasing the surface area of the port faces of the drum accelerator and increasing the discharge angle and discharge radius for the disk accelerator improved the performance of the accelerators.

Keywords

Accelerator, centrifugation, decanter, separation, separator

Date received: 1 January 2014; accepted: 27 May 2014

Introduction

A decanter centrifuge (Figure 1) uses centripetal acceleration to continuously separate a heavier solids phase from up to two lighter liquid phases. The mixture is gravity fed or pumped through a stationary feed tube into the accelerator where it gains some tangential velocity before entering the rotating bowl. The mixture experiences centripetal acceleration within the bowl that causes the denser solids to sediment against the bowl wall. Once the solids have settled, they are transported by the scroll conveyor from the cylindrical section to the conical beach before being ejected through the solids discharge ports. The scroll rotates with a small differential velocity relative to the bowl. The liquid phase flows in the opposite direction to the settled solids to the liquid discharge ports at the end of the cylindrical bowl. A detailed description of a decanter centrifuge is given in earlier works.[1–5]

One of the most important aspects of a decanter centrifuge is the incoming feed being accelerated to the rotational speed necessary for high separation rates. The incoming feed is rotationally accelerated by the accelerator before entering the bowl; if the feed has not reached the solid body rotational speed of the bowl, it is further accelerated within the liquid pool. The acceleration of the feed can consume the largest portion of the total power.[6,7] The acceleration power consists of two components: the kinetic energy of the solids and liquids as they leave their respective discharge ports and an irreversible viscous loss. It was shown in Fainerman and Paramonov[8] that the viscous losses are equal to the gain in kinetic energy. Therefore, a simple relationship for the total power required by acceleration is given by

$$\dot{E}_A = \omega_b^2\left(\dot{m}_S r_{dS}^2 + \dot{m}_L r_{dL}^2\right) \quad (1)$$

where ω_b is the bowl speed, $\dot{m}_L$ the liquid mass flow rate, $\dot{m}_S$ the solid mass flow rate, r_{dL} the liquid

Department of Mechanical Engineering, University of Canterbury, New Zealand

Corresponding author:
George RA Bell, Department of Mechanical Engineering, University of Canterbury, PO Box 4800, Ilam, Christchurch 8041, New Zealand.
Email: george.ra.bell@gmail.com

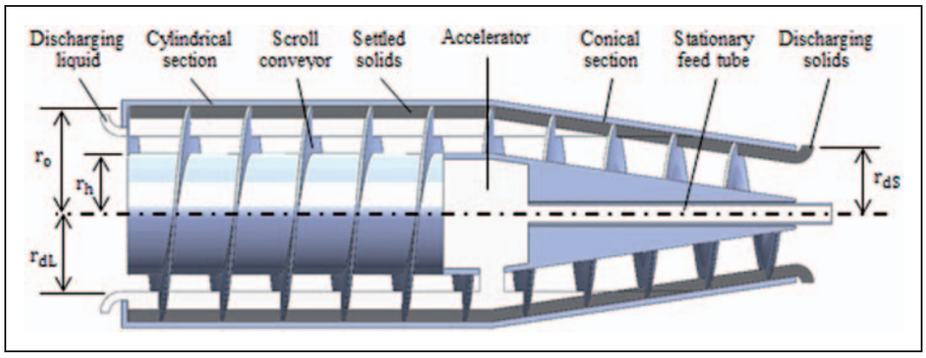

Figure 1. Schematic of a decanter centrifuge processing two phases.

discharge radius and r_{dS} the solid discharge radius. One performance metric for a feed accelerator proposed by Leung[2] is the accelerator efficiency ε_a, which is the ratio of the tangential velocity component of the fluid leaving the accelerator u_θ and the solid body speed at the accelerator discharge radius $r_h\omega_b$

$$\varepsilon_a = \frac{u_\theta}{r_h\omega_b} = \frac{u_\theta}{(D/2)\omega_b} \tag{2}$$

The accelerator efficiency can also be determined by measuring the torque required by the accelerator, where a higher torque results in greater acceleration efficiency; this is due to the torque acting on the accelerator being equal to the rate of change of angular momentum of the fluid with respect to time. Leung[2] presented the following relationship between torque T, mass flow rate $\dot{m}$, rotational speed of the accelerator ω, discharge radius of the accelerator r and accelerator efficiency

$$\varepsilon_a = \frac{T}{\dot{m}\omega r^2} \tag{3}$$

The importance of the feed accelerator is often not appreciated. If the feed is not fully accelerated when it enters the pool, it is detrimental to the operation of the centrifuge. Poor acceleration can result in re-suspension of settled solids, disturbance to the surface of the pool and high wear on the bowl and scroll adjacent to the feed ports.[2,9] If the feed is under accelerated, the magnitude of acceleration will initially be lower and therefore a longer settling length is required to achieve the same separation rate. A more efficient accelerator will provide higher solids recovery and clearer centrate.[9] While the accelerator must increase the rotational speed of the feed, it must not severely increase the radial component. A high radial velocity leads to plunging of the incoming feed into the rotating pool. This can disturb previously settled solids and increase wear on the bowl in the region around the accelerator.

Experimental evaluation was completed by Leung[2,9–11] to verify the performance of his conical accelerator concept. Several machines were fitted with the conical accelerator and all showed improvements in solids recovery, centrate clarity or throughput. Tan et al.[12] completed a computational simulation of a disk accelerator for a two-stage pusher centrifuge, which has similar requirements to a decanter centrifuge. The design was installed in a full-size centrifuge, although conclusive results were not generated due to mechanical failure of the accelerator. There is presently no literature on a computational analysis of the feed accelerator of a decanter centrifuge, which this study aims to address. Fernandez and Nirschl[13] conducted a computational fluid dynamics analysis of the multiphase flow in a solid bowl centrifuge, although the model did not include the accelerator geometry.

Water was the only fluid considered in this study. While decanter centrifuges are able to process a wide variety of materials, the most common suspension medium is water. The components of a mixture will maintain their respective properties and therefore for relatively low solids content the mixture would behave like water. Applications where this may be applicable include industrial wastewater, potable water (0.5–5% solids[14]), drilling mud and dewatering of coal and mine tailings.

The three components of this work are experimental evaluation, computational analysis and a parametric study. It was necessary to experimentally evaluate the feed accelerator performance to validate the computational model. It was not practical to conduct in situ measurements due to the accessibility of the accelerator in a decanter centrifuge; therefore, a test rig was developed to simulate the feed conditions. Experimental evaluation allowed the measurement of the accelerator efficiency, generation of flow visualisations and insight into manufacturing implications of the different feed accelerator designs. Using computational methods to predict accelerator efficiency and assist in visualising the flow is useful as it replaces time-consuming and expensive experiments. Computational analysis also permitted the effects of subtle design changes to be quantitatively assessed in the parametric study. The computational model only

considered the test rig and was not extended to a full-size decanter centrifuge.

Accelerator designs

There are several designs that are commonly used in industrial centrifuges, but there is an absence of literature that presents the differences between them. Six designs were evaluated as part of this study: these were the conical, disk, drum, Esbjerg, plate and modified disk accelerators. The evaluated designs are presented in Figure 2. All accelerators rotate clockwise as viewed on the page and accept the stationary feed tube as shown. All designs, except the conical accelerator, have a cover plate that has been removed from the images below. The description of the geometry is for the model that was manufactured for evaluation.

The conical accelerator with vanes was developed by Leung for the Bird Machine Company.[2,9,11] The design has a high level of complexity due to the vanes with consequent manufacturing implications. The cone angle was 30° from the axis of rotation and the outer diameter was 115 mm. The cone was designed with eight 8-mm high vanes with a discharge angle of 45°. The vanes were set back from the edge of the cone by 5 mm to allow for a smoothening zone as described by Leung.

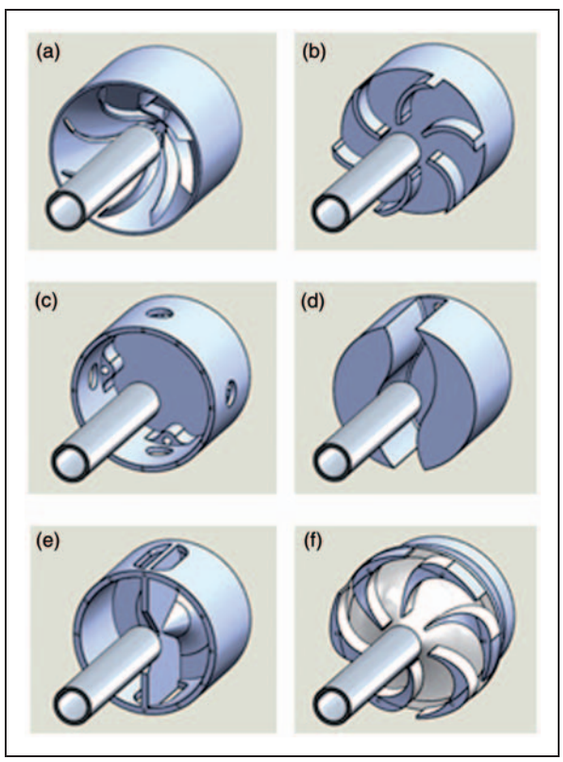

Figure 2. Evaluated accelerator designs: (a) conical, (b) disk, (c) drum, (d) Esbjerg, (e) plate, and (f) modified disk.

The disk accelerator with vanes was also developed by Leung for the Bird Machine Company.[2,15] The design has a medium level of complexity due to the curved vanes and would therefore have some manufacturing complications. There were six 20-mm high vanes. Each vane was 5-mm thick, starting as a radial vane in the centre and curving forwards to a discharge angle of 45° at a diameter of 115 mm. Unlike the conical accelerator, there was no method of flow smoothening.

The drum accelerator is the most common design in decanter centrifuges due to its simplicity and ease of manufacturing. This type of accelerator offers no over speeding. There were four, equally spaced, 20-mm diameter ports on the circumference of the 115-mm diameter cylinder. The wall thickness was 5 mm and the axial internal length was 70 mm.

The Esbjerg accelerator is another common design used by decanter manufacturers. It is a relatively simple design that can be easily incorporated into manufacturing by casting it into the solid scroll conveyor hub. The external diameter was 115 mm and the opening was 25-mm wide and 80-mm long.

The plate accelerator concept is an adaptation of the drum accelerator. The port geometry was changed to slots and a plate was incorporated into the centre to reduce viscous acceleration and increase impulse acceleration. The external diameter was 115 mm. The slots were 12.5-mm wide and 60-mm long. The wall thickness was 5 mm. A cone was added to redirect the flow from an axial to radial direction.

The modified disk accelerator is an adaptation of the disk accelerator made for this study to determine whether greater pool efficiency could be achieved by modifying the design. The vanes were curved to be tangential at the point of discharge, the discharge diameter was increased from 115 mm to 130 mm and a cone was added to aid in the redirection of the flow from axial to radial.

Experimental evaluation

An experimental test rig was designed and constructed that simulated an axial flow entering a rotating bowl on the axis of rotation. The helical scroll was not included in the test rig as it has no effect on the performance of the accelerator. A schematic of the test rig is shown in Figure 3. The rotating bowl was supported at one end and water was fed in through a stationary feed tube at the other. The accelerator was fixed to the rotating bowl. Free-wheeling paddles rotate with the pool and were used to deduce the rotational velocity of the pool. The bowl and rotation meter were housed in a sheet metal enclosure to capture the discharging water. One end could be opened to allow for high-speed photography. The specifications of the test rig are shown in Table 1. A photograph of the assembled test rig is shown in Figure 4. While the test rig has some resemblance to Leung's,[2] it

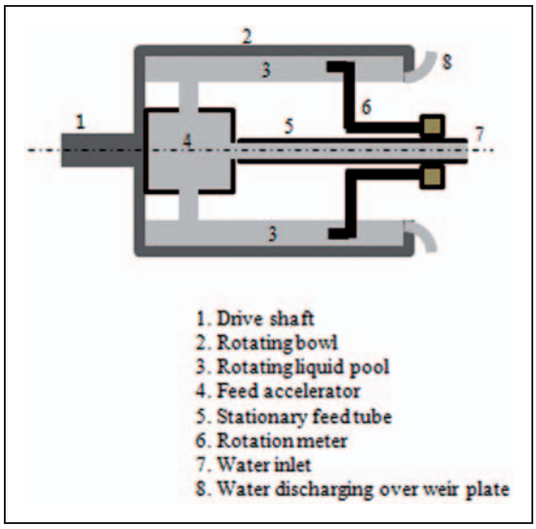

Figure 3. Schematic of the feed accelerator test rig.

5 **Table 1.** Feed accelerator test rig specifications.

Motor power	7.5 kW	Pool ID	180 mm
Bowl speed	1000 r/min	Bowl length	300 mm
Maximum flow rate	40 l/min	Feed tube ID	24 mm
Bowl ID	210 mm	Maximum G-force	117 g

Figure 4. Assembled feed accelerator test rig.

has two key differences. An annular space, which is present in many real decanters, was included between the accelerator and the rotating pool and it was possible to capture images of the flow in the annular space using high-speed photography.

Flow control

A speed-controlled positive displacement pump fed water from a temperature controlled reservoir to a header tank above the rig. The water flowed from the header tank to the stationary feed tube. It was assumed that the water passed through the rig at a constant flow rate. Once the water had passed through the rig, it drained back into the reservoir. The flow rate was carefully measured as a function of the pump's variable speed drive (VSD) frequency. The VSD was able to be set from 0.0 to 50.0 Hz. The setting precision was therefore ±0.2% at the maximum flow rate of 40 l/min and ±2% at the minimum flow rate of 3.4 l/min.

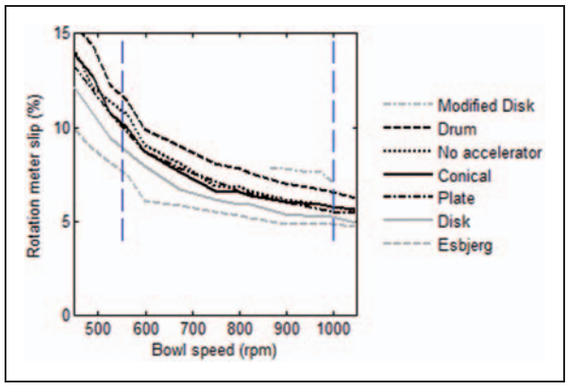

Figure 5. Rotation meter slip as a function of bowl speed. The vertical dashed lines enclose the measured speed range of all accelerator designs.

Speed measurement and control

The pool speed was measured by the rotation meter, which consisted of two paddles mounted on a free-wheeling hub fixed to the feed tube. The paddles protruded 10 mm into the rotating pool. The speed was measured using a double-pass Hall effect sensor. The rotation meter was validated using a handheld optical tachometer. A variation of approximately ±2 r/min was observed in the rotation meter speed.

Slip between the rotation meter and the rotating pool occurred due to aerodynamic drag on the paddles and friction within the bearing. The slip of the rotation meter (s) was measured to determine the correct pool speed. This was achieved by holding the bowl at a constant speed and recording the rotation meter speed ω_r once the steady state was reached for no flow with the bowl full of water. This was based on the assumption that for no water flow the pool attained the solid body rotational speed of the bowl. The slip is expressed as

$$s = \left(1 - \frac{\omega_r}{\omega_b}\right) \tag{4}$$

The slip percentage of the rotation meter was measured for each accelerator design before and after each run for bowl speeds of 450–1050 r/min in 50 r/min increments. The slip for the modified disk accelerator was only measured for bowl speeds between 860 and 1000 r/min due to the smaller range of pool speeds observed for this accelerator. The slip for each accelerator and for no accelerator is presented in Figure 5 for the average value of the

pre- and post-test measurements. Little variation was observed between repeated measurements using the same accelerator. The different slip for each accelerator is possibly due to the stirring effect that the accelerator has on the air within the bowl – this could result in differences in the drag acting on the rotating paddles and the inner surface of the rotating pool.

Accelerator construction

All the accelerators were produced from ABS plastic using a three-dimensional (3D) printer. Printing the designs allowed for the analysis of complex geometries such as the conical and disk accelerators. The surface roughness of the accelerators was approximately 100 μm; the influence of surface roughness was not explored in this study. Each accelerator design, excluding the conical accelerator, had a cover plate fitted over the end with a 40-mm diameter hole to accommodate the feed tube. The feed tube for the conical accelerator was extended as far as possible towards the root of the vanes to ensure that the effect of gravitational droop was negligible. The feed tube terminated at the inner surface of the cover plate for the other accelerators.

Procedure

The same procedure was followed for each accelerator, and all were tested at least twice. The accelerator was fitted into the test rig and bolted in place. The water in the reservoir was heated to 25 °C. The bowl was accelerated to the running speed and filled with water; the rotation meter slip was measured from 450 to 1050 r/min in 50 r/min increments. The bowl speed was then set to 1000 r/min. The water pump was switched on and flow was passed through the rig. The flow rate was increased from 3.4 to 40 l/min in 10 increments. Once the steady state was achieved at each flow rate, the rotation meter speed was recorded. The rotation meter speed was adjusted to account for slip. At the conclusion of the test, the slip was measured again. To give a control value for the accelerator performance, a full test was completed with no accelerator in place. The incoming feed poured out of the feed tube into the rotating bowl with no pre-acceleration.

High-speed photography

High-speed photography allowed for a detailed insight into the subtly different flow patterns within the test rig. The flow conditions as the water left the accelerator and entered the rotating pool were of particular interest. A MotionPro X3 high-speed camera and a 1 kW stage light were employed to capture images of the flow passing between the accelerators and the rotating pool. The surfaces facing the light were painted matte black to reduce reflections and improve image quality. The camera and light were positioned approximately 1 m from the end of the test rig. A frame rate of 900 fps was used. The shutter speed was decreased to the minimum required level to ensure the images did not become blurred. A bowl speed of 1000 r/min and a water flow rate of 30 l/min were used during filming.

Torque measurement

The torque imparted on the water by the feed accelerator was measured in order to quantitatively validate the computational model. The test rig was modified from the original configuration in Figure 3 by removing the bowl and replacing the larger three-phase motor with a smaller DC motor and an epicyclic gearbox. A reaction arm was fixed to the motor and gearbox casing and extended to a 50-N load cell at a radius of 107 mm from the axis of rotation. The modified configuration is shown schematically in Figure 6.

The following procedure was used to measure the torque imparted on the water by the feed accelerator. The load cell was zeroed at 0 r/min. The motor was switched on and the speed was raised to 750 r/min. The speed was held constant until the measured torque reached a steady value. Water was fed into the accelerator through the stationary feed tube and the increase in torque was measured. This procedure

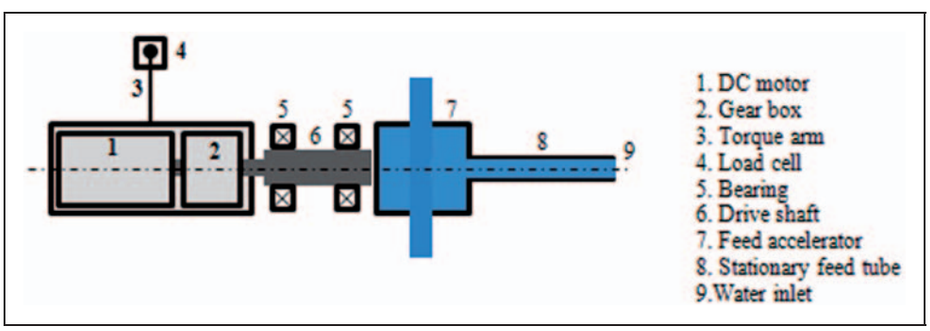

Figure 6. Schematic of the modified test rig for torque measurements.

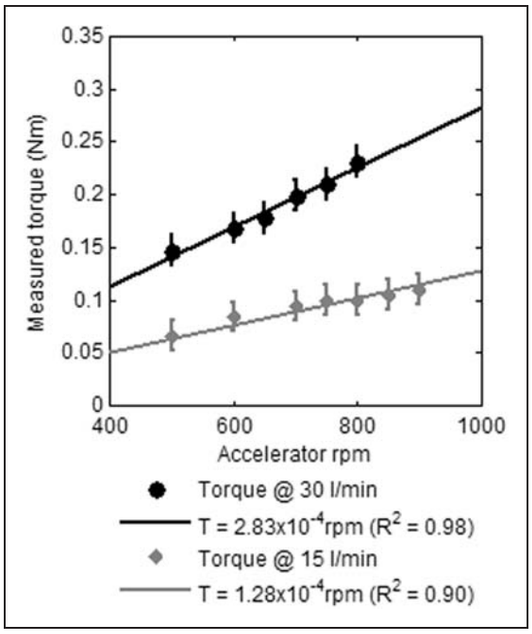

Figure 7. Measured torque as a function of rotational speed for the disk accelerator with water flow rates of 15 and 30 l/min.

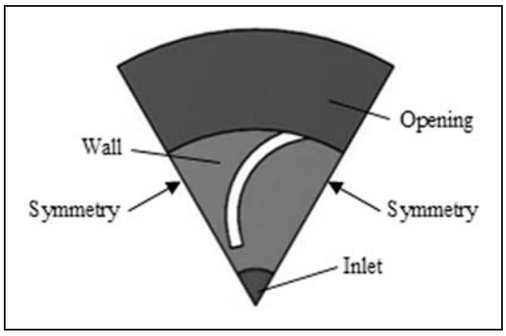

Figure 8. Disk accelerator fluid domain (clockwise rotation).

Table 2. Number of nodes for each accelerator mesh.

Conical	67,608	Esbjerg	165,411
Disk	58,790	Plate	204,204
Drum	156,310	Modified disk	69,264

was repeated multiple times for each design to ensure consistency of the measurements. The influence of the flow rate and rotational speed was partially explored for the disk accelerator. The same procedure was followed as above, except the flow rate and speed were also varied. The torque was measured for a flow rate of 30 l/min of water at a rotational speed of 750 r/min. A speed of 750 r/min was used due to the power limit of the available motor. It was found that the speed was linearly proportional to the torque (Figure 7) and therefore the results were scaled to 1000 rpm to allow for comparison with the computational results.

The torque could be measured within ±0.01 Nm and was considered to be the greatest source of uncertainty – this range of ±0.01 Nm was scaled to ±0.014 Nm at 1000 r/min. The next greatest source of error was the speed control, which was deemed acceptable if the speed was within ±2 r/min.

Computational model

The water flowing through each of the accelerators shown in Figure 2 was simulated using ANSYS CFX 14.5. The flow path and torque induced on the fluid were predicted for each design. The computational model considered a feed accelerator rotating at 1000 r/min, accelerating 0.5 kg/s (30 l/min) of water at 25 °C.

Fluid domain and mesh

The 3D fluid domain included the internal space within the accelerator and the annular space between the accelerator and the inner surface of the rotating pool. Including the annular space allowed for the comparison between the computational results and the high-speed photography. The length of the annular space along the axis of rotation was 60 mm for the conical, disk, drum and modified disk accelerators and 120 mm for the Esbjerg and plate accelerators. The annular space was centred across the discharge ports, except for the conical accelerator where it was offset 20 mm in the direction of flow. The domain did not include the feed tube as it was expected that this would have an insignificant impact on the results. Each of the accelerators possessed a degree of symmetry about the axis of rotation and therefore only a portion of the domain needed to be modelled. The periodic symmetric assumption reduced the number of nodes and solving time. The fluid domain for the disk accelerator is shown in Figure 8.

A patch conforming tetrahedral mesh with boundary inflation was used. Inflation was added to all wall boundaries to ensure that the boundary layer influence was correctly captured. All walls had 10–15 inflation layers with a first layer thickness of 0.2–0.3 mm; at least 10 nodes are required within the boundary layer.[16] The mesh statistics for each accelerator are given in Table 2.

Setup

A steady-state analysis was selected for this model. While there may be some time-dependent effects due to turbulence, the outputs of interest are assumed to be steady state. A multiphase Eulerian model was used in this analysis as it offers complete global information and turbulence can be included. The shear stress transport turbulence model was used with curvature correction; this was chosen as it is suitable

for modelling the turbulent boundary layers that are present in feed accelerators.[17] A homogeneous model was chosen as the relative velocity between the water and air phases is small; also, this allowed for the solution to be reached faster as there are fewer equations to solve.

A rotating domain was used which included both the water being accelerated and the air that was present within the accelerator. Both fluids were set at 25 °C and were considered as continuous fluids. The interface between the water and air was set as a free surface with a surface tension coefficient of 0.073 N/m.

Each accelerator has four types of boundary conditions: inlet, opening, wall and symmetry. The inlet condition for each design was specified as a constant mass flow rate of 0.5 kg/s normal to the boundary; this was reduced depending on the degree of axial symmetry. The inlet was set to be stationary relative to the rotating domain. The Reynolds number for 0.5 kg/s of 25 °C water flowing through a 24-mm diameter pipe is 29,770, resulting in fully turbulent flow. Medium turbulence intensity of 5% was used for the inlet. Openings were used as opposed to outlets because an outlet does not allow for fluid to enter the domain, therefore restricting the circulation of air in the domain. The fluid at the opening was set to be air, which allowed water to exit the domain but only air to enter. A no-slip condition was enforced at the walls of the accelerator. The wall boundary was set to rotate with the domain. An upwind advection scheme was used with a first-order turbulence numeric. A convergence criterion of 1×10^{-4} of the RMS values was used. The timescale was set to automatic and conservative.

Grid independence

To confirm the results were independent of the mesh, the torque was recorded for several models with different meshes. The stated variation is that from the torque calculated when using the maximum number of nodes or inflation layers. There was a 2.6% variation of the torque acting on the disk accelerator when using 33,717 and 58,790 nodes. The drum accelerator was modelled with 58,765–156,310 nodes; when more than 92,882 nodes were used the variation in torque was 5.9%. There was less than a 0.5% variation in the torque acting on the plate accelerator when more than 121,816 nodes were used. The influence of the number of inflation layers was investigated. The drum accelerator was meshed with 5, 8, 10, 15 and 25 inflation layers within the 5-mm near-wall layer. The variation in torque was less than 3.8% when 10 or more layers were used. For 15 inflation layers on the walls of the drum accelerator using the first layer thicknesses of 0.5, 0.4, 0.35, 0.3, 0.25 and 0.2 mm, there was less than 1% variation in the torque.

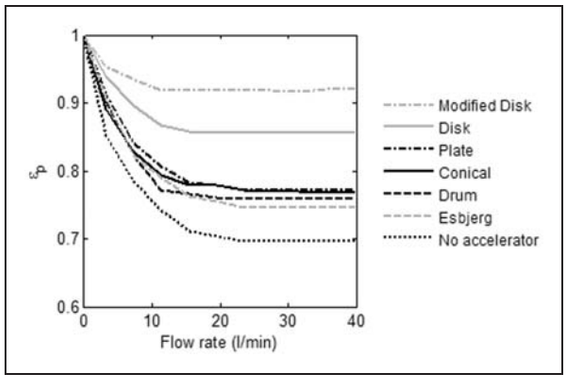

Figure 9. Experimentally measured pool efficiency as a function of flow rate for a bowl speed of 1000 r/min.

Table 3. Experimental results at 30 l/min and 1000 r/min.

Accelerator	Corrected pool speed (r/min)	Pool speed increase (r/min)	ε_p
Conical	769.5	74.0	0.770
Disk	855	159.5	0.855
Drum	757.6	62.1	0.758
Esbjerg	745.5	50.0	0.746
Plate	771.9	76.4	0.772
Modified disk	917	221.5	0.917
No accelerator	695.5	–	0.696

Results

The pool efficiency for each design and the base case where no accelerator was fitted are plotted against flow rate in Figure 9. The pool efficiency ε_p is the ratio of the pool speed ω_p (when corrected for slip) and the bowl speed

$$\varepsilon_p = \frac{\omega_p}{\omega_b} \tag{5}$$

The pool speed and increase over the base case for a flow rate of 30 l/min are given in Table 3 for the experimental trials. The measured and predicted torques are presented in Figure 10 for each of the six designs that were evaluated – the measured torque was scaled from 750 to 1000 r/min. The measured and predicted torques and efficiencies are shown in Table 4. The measured torque as a function of rotational speed for the disk accelerator is shown in Figure 7 for water flow rates of 15 and 30 l/min. The measured torque as a function of the measured increase in pool speed is given in Figure 11. The flow visualisations generated using the computational model and high-speed photography are presented in Figure 12.

Discussion

The experimentally measured pool efficiency and torque, and the computationally predicted torque are in good agreement. The disk and modified disk accelerators exhibited superior pool efficiencies. The modified disk accelerator produced a greater pool efficiency than the other designs due to the larger discharge radius and the greater discharge angle of the vanes. The conical and plate accelerators performed similarly, followed by the drum and Esbjerg accelerators.

It is important to note that the efficiency values presented in Table 4 are the accelerator efficiency (equation (2)). It was initially expected that the modified disk accelerator would have a higher accelerator efficiency than the disk accelerator due to the greater vane discharge angle. This was not observed and was most likely due to greater viscous losses due to the longer length of the vanes. Despite having a lower accelerator efficiency, the modified disk accelerator had a significantly higher pool efficiency due to the larger discharge radius.

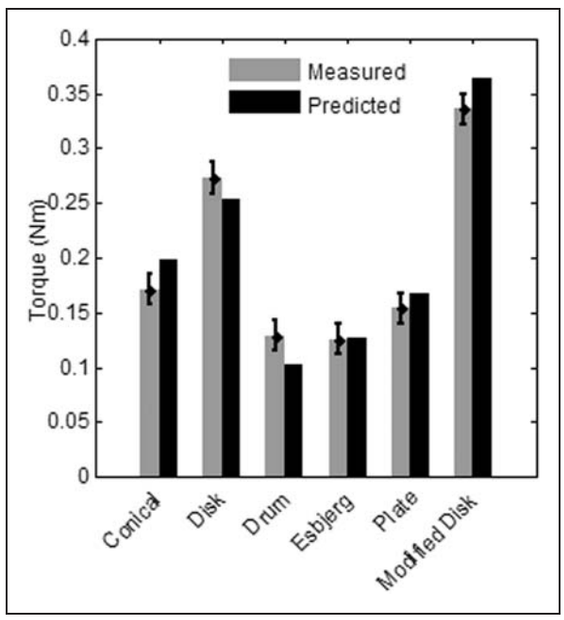

Figure 10. Measured and predicted torque for the six feed accelerator designs with a water flow rate of 30 l/min and bowl speed of 1000 r/min.

The pool efficiencies shown in Figure 9 were higher at lower flow rates due to the longer residence time of the water in the bowl. It is during this time that the viscous forces act on the fluid, inducing rotation.

Figure 10 shows that the predicted torque is in good agreement with the measured torque, thus providing quantitative validation of the computational model. The greatest variation occurred for the conical accelerator, where the predicted torque was 15% greater than the measured value. The computational model under predicted the efficiency of the drum accelerator, this could potentially be due to the mounting bosses not being included in the computational model. The variations between the experimental and computational results were deemed to be acceptable for this study.

Figure 7 clearly shows that the torque is linearly proportional to speed, justifying the assumption that the torque could be scaled from 750 to 1000 r/min. It can also be observed that the volumetric flow rate influences the torque for the disk accelerator. The variation is due to the mass flow-induced velocity component increasing for higher volumetric flow rates. This is well documented by Leung.[2]

Figure 11 shows that the measured torque is linearly proportional to the measured increase in pool speed. Therefore, maximising the torque will result in maximised pool speed, which is ultimately one of the goals of the accelerator. While the data are approximately linear in the region measured, the trend line does not pass through 0, 0. This could either be due to the relationship being non-linear outside the measured range or a finite torque being required to increase the pool speed. This was not explored further as only designs that significantly increase the pool speed were of interest.

The flow visualisation results allowed for qualitative validation of the computational model. The flow paths observed using high-speed photography were similar to the predicted flow paths for all designs. The water only occupied a small portion of the volume inside the conical, disk, plate and modified disk accelerators; the majority of the flow in these

Table 4. Measured and predicted torque and accelerator efficiency for a water flow rate of 30 l/min rotating at 1000 r/min.

Accelerator	Measured torque (Nm)	Predicted torque (Nm)	Measured ε_a	Predicted ε_a	Variation predicted/measured (%)
Conical	0.171	0.198	0.99	1.14	15.2
Disk	0.273	0.254	1.58	1.48	−6.3
Drum	0.129	0.110	0.75	0.64	−14.7
Esbjerg	0.126	0.127	0.73	0.73	0
Plate	0.154	0.167	0.89	0.96	7.9
Modified disk	0.336	0.364	1.52	1.65	8.6

XML Template (2014) [4.6.2014–1:32pm] [1–15]
//blrnas3/cenpro/ApplicationFiles/Journals/SAGE/3B2/PIEJ/Vol00000/140023/APPFile/SG-PIEJ140023.3d (PIE) [PREPRINTER stage]

accelerators occurred in a thin layer on the internal surfaces. The flow visualisations agreed well with the efficiency results for each design. The disk and modified disk accelerators were the only designs that showed any over speeding of the water as it left the accelerator; this gave rise to their high efficiencies when compared to the other designs. The concentration of the incoming feed could also be observed. The drum and Esbjerg accelerators appeared to have relatively dispersed flow, while the conical, disk, plate and modified disk accelerators had somewhat concentrated flow streams. The depth of disturbance could not be observed.

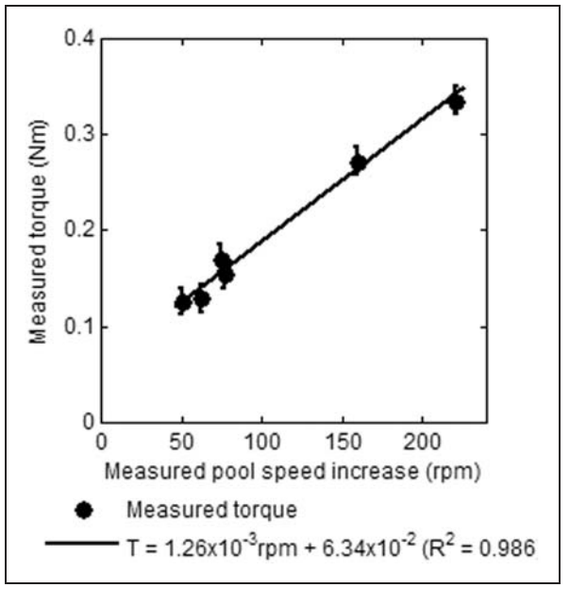

Figure 11. Measured torque as a function of the measured increase in pool speed for a water flow rate of 30 l/min and a bowl speed of 1000 r/min.

The experimental method did not offer a quantifiable means of comparing the radial velocity for different accelerator designs. Further analysis could include a study into the quantification and effect of pool penetration. Some anomalies occurred in the computational model for several of the designs. The computational results for the plate accelerators predicted that a small amount of water would be discharged from the leading edge; this was not present in the experimental results. Smearing between the air and water phases was observed in some regions of the flow; this was likely to be due to insufficient mesh refinement at the free surface. The mesh was not refined further as the smearing primarily occurred in the annular space and satisfactory agreement was reached between the measured and predicted torque values.

Parametric study

None of the accelerators that were analysed were optimised prior to the analysis. The dimensions selected

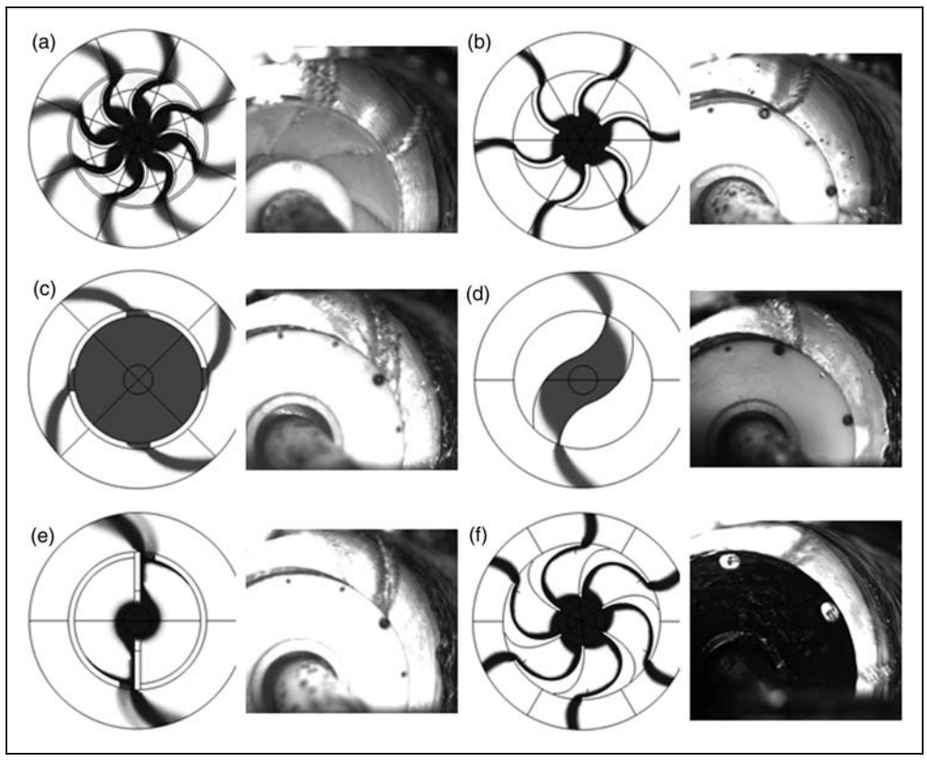

Figure 12. Axial view of the flow within and around the feed accelerator, predicted using ANSYS CFX and captured using high-speed photography: (a) conical, (b) disk, (c) drum, (d) Esbjerg, (e) plate, and (f) modified disk.

were based on the proportions observed in industrial decanters. A parametric study of the disk and drum accelerators was undertaken to pursue an optimal design of each and to gain an understanding of the effect of each parameter. The disk and modified disk accelerators were proven to be the best performing accelerator designs of the six that were tested. Despite its poor performance, the drum accelerator was selected for further analysis as it is the most commonly used design and cheapest to manufacture.

It has been shown that the torque acting on the accelerator walls, predicted using the computational model, is a good indicator of the relative performance of an accelerator design. This knowledge was applied in this work by varying parameters of the disk and drum accelerators and predicting the influence they have on the torque induced on the fluid being accelerated. A base case for all parameters was chosen for each accelerator and each parameter was then varied independently. The torque was converted to the accelerator efficiency using equation (3) and the discharge radius of the accelerator.

Using a computation package such as ANSYS-CFX to conduct this analysis significantly reduced the number of experiments that were required. Twenty-five runs were completed for the disk accelerator and 18 for the drum accelerator. This would have required 43 different accelerators to be manufactured and tested.

The computational model was adapted for this analysis. The domain was reduced to only include the fluid within the accelerator and not the fluid in the annular space between the accelerator and the rotating pool; this was justified as only the torque acting on the accelerator walls was required. Period symmetry and a rotating domain were used; the angle of periodicity varied depending on the number of ports or vanes.

Drum accelerator analysis

The values for each parameter are given in Table 5. The base design for the drum accelerator are the values in bold. The base values were held constant while one parameter was varied. The drum accelerator is shown in Figure 13 with the dimensions that were varied. A stand-off tube is an extension tube added to the accelerator ports.

The torque and hence accelerator efficiency due to the port faces and the inner surface of the drum were extracted from the computational model. The port faces and inner surface correspond to impulse- and viscosity-induced torque, respectively.

The effect that the port diameter has on the accelerator efficiency is shown in Figure 14(a). The majority of the accelerator efficiency, 80–85%, is due to the port faces. As the port diameter is increased the viscous component remains relatively unchanged, while the component due to the port faces increases. Increasing the port diameter is a simple and effective measure to increase the accelerator efficiency.

Adding additional ports is also an easy method of increasing the surface area of the port faces. From Figure 14(b), it can be seen that it is desirable to have at least six ports as there is a notable gain in the accelerator efficiency. The component supplied by the inner surface remains relatively constant. The observed increase arises from the increasing component from the port faces.

The effect of varying the wall thickness is shown in Figure 14(c). The wall thickness was increased inwards so the discharge radius was not changed. As the wall thickness increased, the viscous component decreased due to the smaller radius and surface area of the inner faces of the drum. As the thickness increased, the surface area of the port faces increased resulting in a significant rise in the component applied by the port faces.

A port stand-off tube is an easy way of increasing the discharge diameter and the apparent wall thickness. The effect of adding a 5- and 10-mm stand is shown in Figure 14(d). The calculation of the accelerator efficiency included the increase in the discharge radius due to the stand-off tube. A significant increase in the accelerator efficiency was observed with the addition of either stand.

While the effect of varying viscosity has not been quantified, it is expected that the torque, and hence accelerator efficiency, would increase for the drum accelerator with increasing viscosity. This is due to

Table 5. Parameter values for the drum accelerator.

Port diameter (D_p)	5, 10, 15, **20**, 25, 30, 40, 50 mm
Number of ports	2, **4**, 6, 8
Wall thickness (t_w)	2, **5**, 10, 15, 20, 25 mm
Stand-off tube height (h_s)	**0**, 5, 10 mm

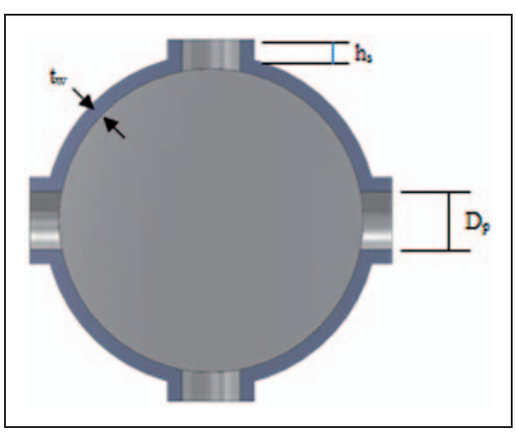

Figure 13. Drum accelerator dimensions.

XML Template (2014) [4.6.2014–1:32pm] [1–15]
//blrnas3/cenpro/ApplicationFiles/Journals/SAGE/3B2/PIEJ/Vol00000/140023/APPFile/SG-PIEJ140023.3d (PIE) [PREPRINTER stage]

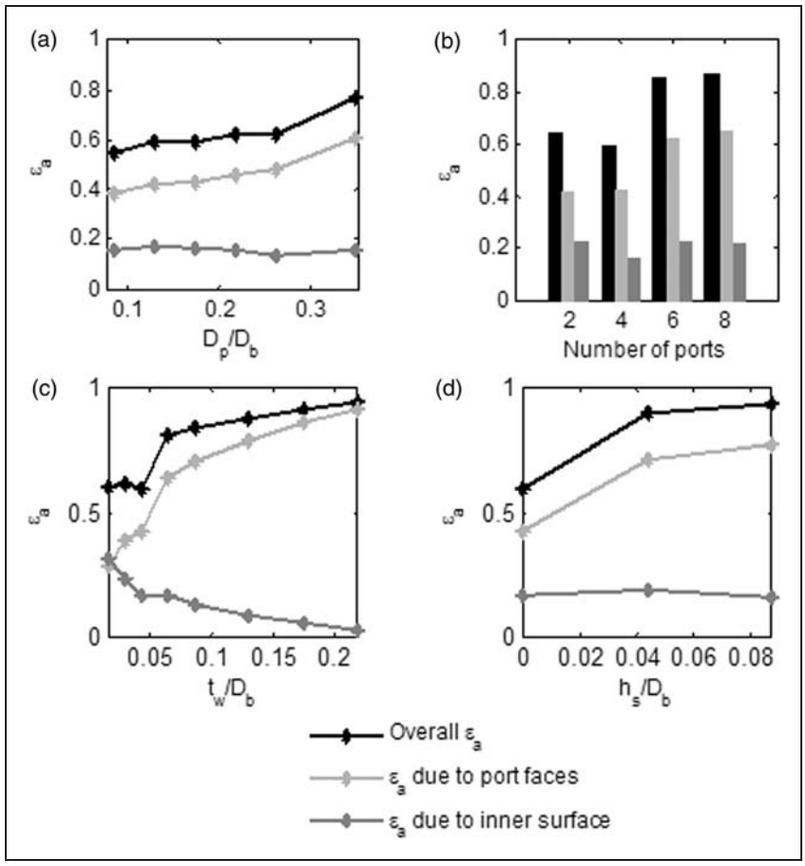

Figure 14. Drum accelerator efficiency and a function of (a) port diameter, (b) number of ports, (c) wall thickness and (d) stand-off tube height.

Table 6. Parameter values for the disk accelerator.

Vane discharge angle (A)	0°, 22.5°, **45°**, 67.5°, 90°
Number of vanes	2, 4, **6**, 8
Discharge radius (D)	**115**, 125, 135, 145, 155 mm
Disk thickness (L_v)	5, 10, **20**, 30, 40 mm
Mass flow rate	0.25, **0.5**, 1, 1.5, 2, 3 kg/s
Rotational speed	500, **1000**, 1500, 2000, 2500 r/min

an expected increase in the component of accelerator efficiency due to the inner surface of the accelerator.

Disk accelerator analysis

The values for each parameter are given in Table 6. The base design for the disk accelerator are the values in bold. The base values were held constant while one parameter was varied. The disk accelerator is shown in Figure 15 with the dimensions that were varied.

The effect the vane angle has on accelerator efficiency is shown in Figure 16(a). The improvement from increasing the vane angle arises from the utilisation of the mass flow-induced velocity to over speed the fluid. Significant improvements were observed up to a vane angle of approximately 70°; beyond this angle, the rate of gain decreases.

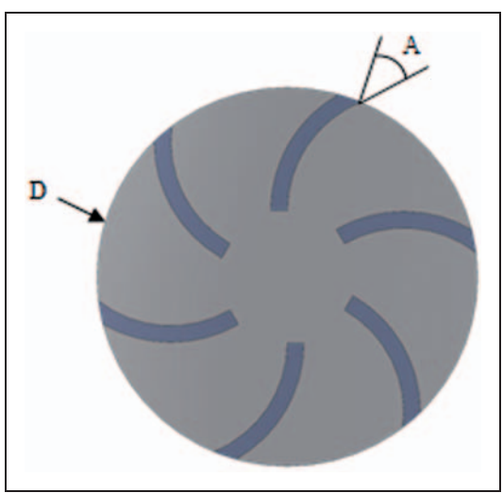

Figure 15. Disk accelerator dimensions, L_v = vane height out of page.

From Figure 16(b), it can be seen that the number of vanes had little effect on the accelerator efficiency. When the number of vanes is increased, the thickness of the water stream on each vane decreases, therefore

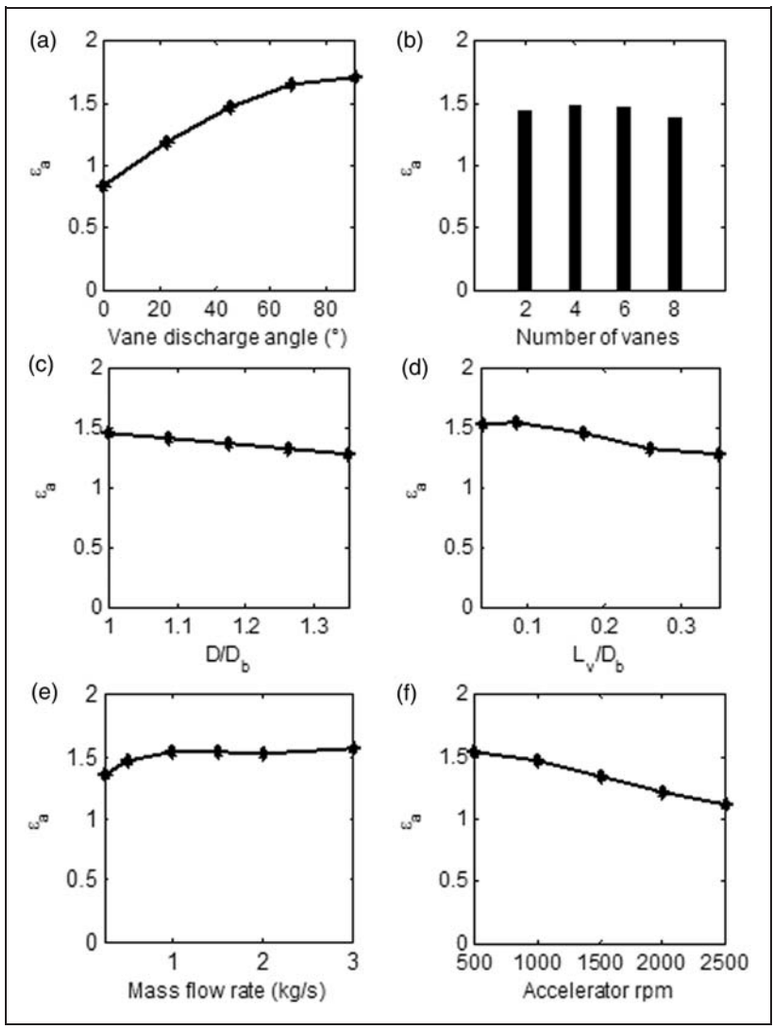

Figure 16. Disk accelerator efficiency: (a) vane discharge angle, (b) number of vanes, (c) discharge radius, (d) disk thickness, (e) mass flow rate and (f) rotational speed.

decreasing the torque applied by each vane. As the thickness of the water passing over each vane decreases, a larger portion of the flow moves into the wall layer, increasing the viscous losses and decreasing the acceleration capability, although this only has a small effect over the range of the number of vanes analysed.

The relationship between discharge diameter and accelerator efficiency is shown in Figure 16(c). The calculation of the accelerator efficiency included the variation of the discharge radius. While it is shown here that increasing the discharge diameter decreases the accelerator efficiency, this is outweighed by the higher tangential velocity. Increasing the discharge radius is an easy and effective method of improving the performance of the disk accelerator. The decrease in accelerator efficiency is most likely due to the higher viscous losses for a longer vane.

Figure 16(d) shows that increasing the depth of the vanes beyond $L_v/D_b = \sim 0.1$ is detrimental to the accelerator efficiency. Increasing the vane depth has a similar effect to adding extra vanes where the thickness of the flow is decreased. Again, this causes a greater portion of the flow to be in the wall layer, therefore decreasing accelerator performance.

Figure 16(e) shows the effect the mass flow rate has on the accelerator efficiency. The accelerator efficiency is approximately constant, except at lower flow rates where the efficiency decreases. This variation is due to the mass flow-induced velocity component being larger and the decreased portion of the flow within the boundary layer travelling along the vanes for high flow rates.

The rotational speed versus accelerator efficiency is shown in Figure 16(f). The accelerator efficiency decreases linearly with rotational speed. This could be due to multiple factors: one being the reduced relative size of the mass flow-induced velocity and the other being increased turbulence.

Conclusions

The disk and modified disk accelerators exhibited the highest accelerator and pool efficiencies among the designs that were evaluated. The next best performing designs were the conical and plate accelerators, followed by the drum and Esbjerg accelerators. The computational and experimental results agreed that the disk and modified disk accelerators were better at rotationally accelerating the incoming fluid. The agreement between the computational and experimental results allowed for further use of the computational model in the parametric study of the disk and drum accelerators. The parametric study revealed the influence that each of the important design parameters for the drum and disk accelerators had on the accelerator efficiency. The port diameter, number of ports, wall thickness and effect of a stand-off tube were examined for the drum accelerator. It was found that increasing the port face area by any means improved the accelerator efficiency. This could be achieved by increasing the port diameter, adding additional ports, increasing the wall thickness or adding a stand-off tube. The vane discharge angle, number of vanes, discharge radius, vane depth, mass flow rate and speed were examined for the disk accelerator. It was found that increasing the discharge diameter, vane angle and thickness of the flow along each vane improved the performance.

Several conclusions regarding the design of the accelerator can be drawn from this analysis:

1. Adding a feature to the geometry of the feed accelerator to induce over speeding, such as forward curving vanes, can significantly improve the accelerator efficiency of a design.
2. Increasing the discharge radius of the accelerator significantly improves the accelerator efficiency.
3. Features should be included in the design that imparts an impulse force/pressure on the fluid as viscous dissipation is a poor mechanism for acceleration.

The findings from this work can be used in the design and development for any application that requires fluid to undergo rotational acceleration.

Funding

This research received no specific grant from any funding agency in the public, commercial, or not-for-profit sectors.

Conflict of interest

The authors declare no competing financial interest.

Acknowledgement

This work was completed with the assistance of Bellmor Engineering Ltd, with a Fellowship from the New Zealand Ministry of Science and Innovation.

References

1. Records A and Sutherland K. *Decanter centrifuge handbook*. ▮▮: Elsevier, 2001.
2. Leung WWF. *Industrial centrifugation technology*. New York: McGraw-Hill, 1998.
3. Leung WW-F. *Centrifugal separations in biotechnology*. Oxford: Elsevier, 2007.
4. Corner-Walker N and Records FA. The dry solids decanter centrifuge: conveyor torque and differential. *Filtr Sep* 2000; 37: 18–23.
5. Stahl WH. *Industrie-Zentrifugen*. Männedorf: DrM Press, 2004.
6. Bell GRA, Symons DD and Pearse JR. Mathematical model for solids transport power in a decanter centrifuge. *Chem Eng Sci* 2014; 107: 114–122.
7. Reif F and Stahl W. Transportation of moist solids in decanter centrifuges. *Chem Eng Prog* 1989; 85: 57–67.
8. Fainerman IA and Paramonov IA. Calculation of the power of centrifuge drives required for the acceleration of suspensions. *Chem Petrol Eng* 1985; 21: 184–186.
9. Leung WWF and Shapiro AH. Improved design of conical accelerators for decanter and pusher centrifuges. *Filtr Sep* 1996; 33: 735–738.
10. Leung WWF and Shapiro AH. Feed accelerator system including accelerating vane apparatus. Patent 5380266, USA, 1996.
11. Leung WWF and Shapiro AH. Feed accelerator system including accelerator cone. Patent 5527258, USA, 1995.
12. Tan W, Qiao L, Sha E, et al. Optimal design of the accelerator disk in a two-stage piston pusher centrifuge using numerical simulation. *Ind Eng Chem Res* 2012; 51: 4632–4642.
13. Fernandez XR and Nirschl H. Multiphase CFD simulation of a solid bowl centrifuge. *Chem Eng Technol* 2009; 32: 719–725.
14. Stevenson DG. A review of current and developing potable water treatment processes. *Proc IMechE, Part E: J Process Mechanical Engineering* 2003; 217: 11–23.
15. Leung WWF and Shapiro AH. Efficient double-disc accelerator for continuous-feed centrifuges. *Filtr Sep* 1996; 33: 819–823.
16. LEAP Support Team. *Inflation layer meshing in ANSYS*. ▮▮: Australia, 2012.
17. Menter FR. Two-equation eddy-viscosity turbulence models for engineering applications. *AIAA J* 1994; 32: 1598–1605.

Appendix 1

Notation

D	accelerator discharge diameter
ε_a, ε_p	accelerator, pool efficiency
D_b	base accelerator diameter
ω_b, ω_r, ω_p	bowl, rotation meter, liquid pool angular velocity
r_{dL}, r_{dS}, r_h, r_o	liquid discharge, solids discharge, hub radius, inner bowl radius
$\dot{m}_L$, $\dot{m}_S$	liquid, solid mass flow rate
D_p	port diameter for drum accelerator

$\dot{E}_A$	power consumed by feed acceleration
Re	Reynolds number
s	rotation meter slip
h_s	stand-off tube height of drum accelerator
L_v	vane depth for disk accelerator
A	vane discharge angle from normal
t_w	wall thickness of drum accelerator